NANO LETTERS

pubs.acs.org/NanoLett
Letter

Electrically Controlled Bimetallic Junctions for Atomic-Scale Electronics

Anil Kumar Singh, Sudipto Chakrabarti, Ayelet Vilan, Alexander Smogunov, and Oren Tal*

Cite This: *Nano Lett.* 2023, 23, 7775−7781

ABSTRACT: Forming atomic-scale contacts with attractive geometries and material compositions is a long-term goal of nanotechnology. Here, we show that a rich family of bimetallic atomic-contacts can be fabricated in break-junction setups. The structure and material composition of these contacts can be controlled by atomically precise electromigration, where the metal types of the electron-injecting and sink electrodes determine the type of atoms added to, or subtracted from, the contact structure. The formed bimetallic structures include, for example, platinum and aluminum electrodes bridged by an atomic chain composed of platinum and aluminum atoms as well as iron−nickel single-atom contacts that act as a spin-valve break junction without the need for sophisticated spin-valve geometries. The versatile nature of atomic contacts in bimetallic junctions and the ability to control their structure by electromigration can be used to expand the structural variety of atomic and molecular junctions and their span of properties.

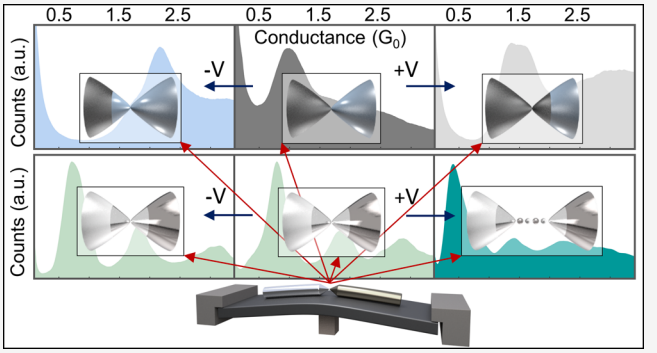

KEYWORDS: *atomic contact, alloy, atomic chain, molecular junction, break junction, electromigration*

Mechanically controllable break junctions (MCBJs; Figure 1a (I)) are a powerful technique, in which a contact between two metal wires is broken to form two electrodes with tips that can be brought together to make an atomic or molecular junction, when molecules are introduced between the electrodes. This technique has been used to study electronic transport at the limit of miniaturization, with the advantage of fast repeated formation and characterization of large ensembles of atomic and molecular junctions.[1−6] Metallic MCBJs are typically based on two electrode tips made of the same metal with rare exceptions, such as the work of Scheer et al., where superconducting electrode tips (Al) bridged by a thin layer of a normal metal (Au) were used for the study of electronic transport in Au atomic contacts.[7,8] Alternatively, bimetallic atomic contacts formed in scanning tunneling microscopes (STMs) by pressing one metal into another were reported two decades ago, revealing that a W or Ni tip indented into a Au substrate can be wetted by Au atoms.[9−12] Although STM tip wetting by different metals has become a common practice, the early works have not been followed by further experimental studies of the structure and composition of atomic-scale contacts that are formed when two different metals are pressed together. These bimetallic structures are attractive because they can increase the structural richness of nanoscale systems in which phenomena related to electronic transport and nanomaterials can be revealed and studied.

Here, using an MCBJ setup, we find that two different metal electrodes (Au−Ni, Al−Pt, and Fe−Ni) that are pushed one against the other and then pulled back can form bimetallic atomic-scale contacts with a rich structural variety. The bimetallic structures include atomic chains composed of two types of atoms, an electrode of one metal ending with an atomic tip or even an atomic chain made of a different metal, and an atomic-scale spin valve based on repeated formation of atomic contacts between two different ferromagnets (see illustrations in Figure 1a (II)). Interestingly, the metallic composition and atomic configuration of the fabricated bimetallic structures can be modified by applying voltage pulses, where the voltage polarity dictates which type of atoms will be added or subtracted from the contact (illustrated in Figure 1a (II), bottom). We further suggest that the relative hardness of the two metals in use affects the nature of the formed structures and their response to voltage pulses. Bimetallic junctions have the potential to extend the structural variety and the wealth of properties that are demonstrated by atomic junctions, as well as by molecular junctions, since the latter can be formed by introducing molecules into bimetallic junctions.

Received: February 8, 2023
Revised: August 13, 2023
Published: August 21, 2023

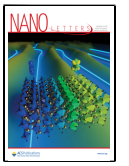

https://doi.org/10.1021/acs.nanolett.3c00508
Nano Lett. 2023, 23, 7775−7781

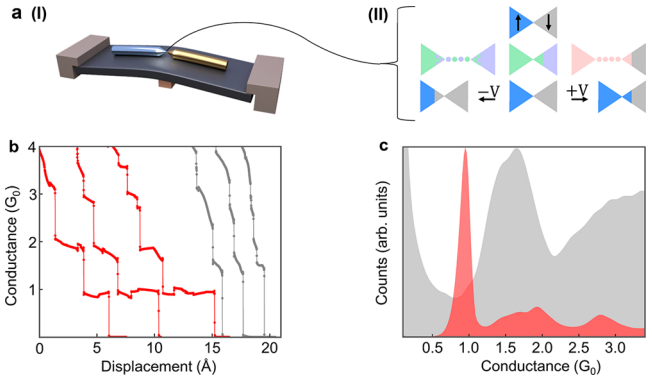

Figure 1. Schematics of a bimetallic break junction and conductance measurements. (a) Schematic illustration of bimetallic junctions prepared in a break-junction setup (I), and schemes (II) of an atomic-scale spin valve (top), bimetallic atomic chain (center left), metallic tip ended with other metal apex (center middle), and monometallic atomic chain suspended between different metal tips (center right) as well as atomic electromigration control over the contact composition (bottom). Each color represents a different metal type. (b) Examples for traces of conductance versus interelectrode displacement for Au−Au junctions (red) and Ni−Ni (gray) monometallic junctions. (c) Conductance histograms based on 10,000 conductance-displacement traces (as seen in b) for Au−Au and Ni−Ni junctions. The peaks indicate the most probable conductance of the atomic-scale contacts during their elongation. The measurements were done at 100 mV applied voltage.

The goal of this Communication is to report on the structural versatility of atomic contacts formed in bimetallic junctions and their tunability thanks to atomically precise electromigration. Combining the properties of different metals in a single atomic-scale structure opens the door for the use of these systems as an advanced testbed for the study of charge, spin, and heat transport as well as material properties, including proximity effects in atomic structures, nanoscale electromigration, and atomic-scale alloying. Our findings raise questions related to structural, mechanical, and electronic properties of bimetallic atomic contacts that will not be addressed here and call for follow-up studies.

The studied bimetallic contacts are prepared in MCBJ setups (Figure 1a (I)). A flexible substrate is first bent. Then, two wire segments (electrodes) made of different metals, each with a sharp tip, are attached to the bent substrate, with their tips pointing to each other. Next, the substrate is relaxed to its flat configuration, and the tips are squeezed against each other to form a macroscale contact. This break junction is placed in a vacuum chamber and cooled to 4.2 K. To prepare an atomic-scale contact, the substrate is bent at its center by a piezoelement that pushes it against two stoppers. Consequently, the tips are pulled apart, and the contact cross-section is gradually reduced until a contact with a single-atom diameter is formed between the electrodes. Further stretching breaks the junction. A new atomic contact can be prepared by relaxing the substrate, such that the electrode tips are pushed against each other to have a multiatomic contact, then the electrodes are pulled apart to reform a single-atom contact. This process can be repeated thousands of times to study ensembles of junctions with different atomic-scale configurations. During the repeated rupture-formation process, the junction's conductance (current/voltage) is recorded as a function of interelectrode distance (Supporting Information, section 1). The repeated squeezing and stretching promote junction cleaning from adsorbed contamination on the initially prepared tips. This is verified by conductance analysis, as detailed below, and in Supporting Information, section 2.

Starting with homometallic junctions, where a single wire is broken and reformed in cryogenic vacuum, Figure 1b presents conductance traces as a function of interelectrode displacement during stretching of Au−Au (red) and Ni−Ni (gray) junctions. The conductance drops in steps whenever the contact diameter between the electrodes is reduced, and the last plateau before junction rupture indicates the conductance of a single-atom contact.[13−18] Since the conductance characteristics can vary between different contact realizations, Figure 1c shows conductance histograms, based on 10,000 conductance traces, each with peaks that identify the most probable conductance during junction stretching. The repeated plateaus seen in Figure 1b for single-atom contacts at ∼1 G_0 for Au−Au junctions and ∼1.6 G_0 (sometimes also at ∼1.2 G_0[16−20]) for Ni−Ni junctions construct dominant peaks in the respective Figure 1c histograms ($G_0 \cong 1/12.9$ (kΩ)$^{-1}$ is the conductance quantum). The ∼1 G_0 conductance of single Au−Au atomic contacts is mostly given by an almost fully open conduction channel, dominated by the s valence orbitals of Au.[7,21] The higher conductance of single Ni−Ni atomic contacts comes from several partially open conduction channels, associated with s, p, and d valence orbitals.[22−24] Other features seen at higher conductance are related to multiatomic contacts. The different shapes of the conductance histograms seen in Figure 1c can therefore be used to distinguish between the formation of Au−Au and Ni−Ni atomic-scale contacts.

We now turn to examine bimetallic junctions based on three metal pairs, Au−Ni, Al−Pt, and Fe−Ni, which are different in their relative hardness (Au ≪ Ni, Al < Pt, Fe≅Ni,[25] see Supporting Information, Table S1). Within each pair, each metal forms junctions (e.g., Au−Au or Ni−Ni junctions in the first pair) that have a different histogram shape (e.g., Figure 1c). Figure 2a I−III presents a typical histogram for Au−Ni bimetallic junctions, together with histograms for Au−Au and Ni−Ni junctions for convenient comparison. The Au−Ni histogram is essentially identical to the Au−Au histogram, indicating that although the two electrodes are made of different metals, the atomic-scale constriction of the junction that dominates its conductance is made of Au (illustrated in Figure 2a II, inset). The formation of pure Au atomic chains during the stretching of Au−Ni junctions with a typical Au−Au interatomic distance further supports this conclusion (see details below). Note that Egle et al. produced by lithographic processing Au−Co−Au and Co−Au−Co break junctions with a central Co or Au section between the outer Au or Co electrodes, respectively. They report the formation of Co−Co and Au−Au contacts in the first case and Au−Au contacts in the second case when the junction is broken and reformed, perhaps consistent with a preference for Au wetting of a harder metal as Co.[26] Figure 2b I−III reveals that the histogram of Al−Pt junctions is similar to that of Al−Al junctions but differs from that of Pt−Pt junctions. Therefore, for Al−Pt junctions, the Pt electrode is covered with Al atoms, forming a monometallic Al contact (illustrated in Figure 2b II, inset). In contrast to the mentioned two cases, where one metal wets the other, Figure 2c I−III shows that the histogram of Fe−Ni significantly differs from that of Fe−Fe and Ni−Ni junctions, indicating the formation of atomic contacts that contain both metals (illustrated in Figure 2c II, inset). Our calculations in Supporting Information section 3 ascribe the lower con-

https://doi.org/10.1021/acs.nanolett.3c00508
Nano Lett. 2023, 23, 7775−7781

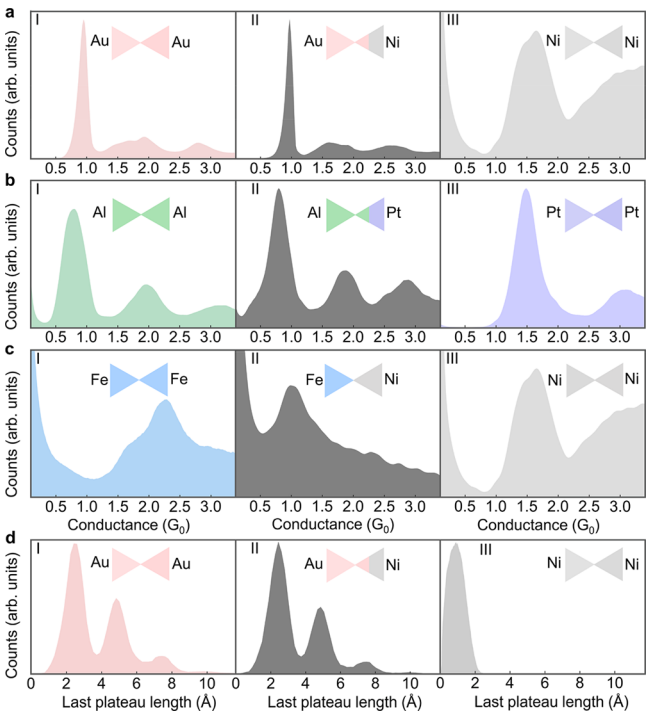

Figure 2. Conductance and length histograms of monometallic and bimetallic atomic-scale junctions. (a) Conductance histograms of Au−Au (I), Au−Ni (II), and Ni−Ni (III) junctions. (b) Conductance histograms of Al−Al (I), Al−Pt (II), and Pt−Pt (III) junctions. (c) Conductance histograms of Fe−Fe (I), Fe−Ni (II), and Ni−Ni (III) junctions. The insets schematically illustrate the metallic composition of the formed atomic contacts in view of the histograms and the described analysis in the text. (d) Length histograms of Au−Au (I), Au−Ni (II), and Ni−Ni atomic-scale junctions. The average interpeak distance between the first three peaks in I and II is 2.5 ± 0.2 and 2.5 ± 0.3 Å, respectively. Each histogram is based on 10,000 conductance-displacement traces, taken during junction elongation at 100 mV applied voltage. Length histograms consider data in the main conductance peak range (0.7−1.1 G_0 for I and II and 1.0−2.0 G_0 for III).

ductance of the main peak in the Fe−Ni histogram (∼1.0 G_0) with respect to the main peaks of the Fe−Fe and Ni−Ni histograms to an abrupt Fe−Ni atomic contact or the formation of an alloy in the contact. For the Fe−Ni junction, the comparable hardness of the two metals most likely suppresses a dominant wetting of one metal tip by the other metal, whereas for Au−Ni and Al−Pt junctions, the softer metal (Au and Al, respectively) constructs the atomic contact by wetting the harder metal (Ni and Pt, respectively).

Coming back to the case of Au−Ni atomic junctions, while it is known that elongation of Au−Au junctions can form suspended atomic chains between the electrodes,[14] elongating Ni−Ni junctions does not form such chains. Figure 1b shows that the last ∼1 G_0 conductance plateau that is associated with the elongation of a Au−Au single-atom contact can have different lengths. Collecting the number of times that a certain ∼1 G_0 plateau length was found in 10,000 traces gives the length histogram presented in Figure 2d (I). This histogram reflects the relative probability of finding an atomic contact with a certain length. The set of peaks is a known fingerprint for the formation of atomic chains with a different number of atoms, whereas the average distance between the peaks is a good measure for the average Au−Au interatomic distance in the elongated chain.[27−29] Here, it is 2.5 ± 0.2 Å for the first three peaks. Interestingly, the elongation of Au−Ni atomic-scale junctions produces an identical length histogram (Figure 2d (II)), with an average interpeak distance between the first three peaks of 2.5 ± 0.3 Å. This indicates that chains made of Au atoms with no Ni or other contaminants are formed in the junctions. Note that the incorporation of foreign atoms (e.g., oxygen) in atomic chains alters the interpeak distances.[20,30] Finally, Figure 2d (III) shows that Ni−Ni does not form atomic chains. As mentioned, wetting a metal tip with Au is a known process. However, the formation of suspended Au atomic chains attached to a different metal, Ni in our case, is an unknown structure. This structure can be used, for example, for the study of magnetic proximity effects in Au atomic chains.

The application of a voltage pulse of +1 or −1 V for 200 μs allows control over the structure and composition of the studied bimetallic atomic contacts and even promotes the formation of new structures. Here as well, we suggest that the relative hardness of the metals may play an important role. As shown in Figure 3a, the application of a voltage pulse does not

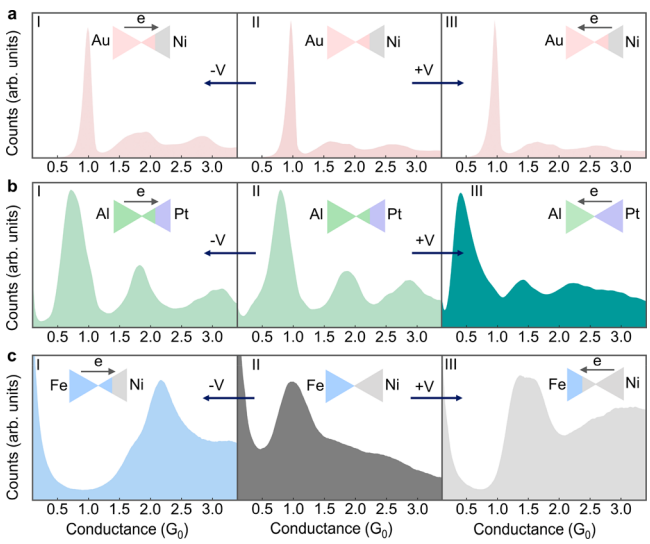

Figure 3. Conductance histograms of bimetallic atomic-scale junctions before and after the applied voltage pulse. (a) Conductance histogram of Au−Ni atomic-scale junctions, after the application of a negative voltage pulse (I), before the application of a voltage pulse (II), and after the application of a positive voltage pulse (III). (b) Conductance histogram of Al−Pt atomic-scale junctions, after the application of a negative voltage pulse (I), before the application of a voltage pulse (II), and after the application of a positive voltage pulse (III). (c) Conductance histogram of Fe−Ni atomic-scale junctions, after the application of a negative voltage pulse (I), before the application of a voltage pulse (II), and after the application of a positive voltage pulse (III). The voltage pulse magnitude is 1 V, and it is applied for 200 μs to a junction with a 3 G_0 conductance (preadjusted by changing the inter electrode distance) before taking the histograms. Each histogram is based on 10,000 conductance-interelectrode displacement traces, taken during junction elongation at an applied voltage of 100 mV.

alter the histograms of Au−Ni junctions. However, repeating the procedure for Al−Pt junctions (Figure 3b) leads to interesting behavior. When the pulse is negative, as when electrons are injected from the Al electrode, no change in the histogram is seen. Following a positive voltage pulse, where the electrons are injected from the Pt electrode, the histogram is

https://doi.org/10.1021/acs.nanolett.3c00508
Nano Lett. 2023, 23, 7775−7781

clearly modified, having a dominant peak at ~0.45 G_0 that is lower than the conductance of a single-atom contact in Al−Al or Pt−Pt junctions. The distinct conductance indicates the formation of atomic-scale contacts that involve both Pt and Al atoms. As will be shown, this contact can be elongated to an atomic chain made of Al and Pt atoms. Our calculations in the Supporting Information, section 3, further relate the low conductance to chain formation.

Figure 3c presents Fe−Ni histograms before and after the application of a voltage pulse. Both positive and negative pulses led to clear histogram modifications. When electrons are injected from the Ni electrode (+1 V pulse), the resulting histogram is similar to that of a Ni−Ni junction. Namely, the atomic Fe−Ni contact was replaced by a Ni−Ni contact (the Fe electrode ends with a tip of Ni atoms). When electrons are injected from the Fe electrode (−1 V pulse), the obtained histogram is similar to that of an Fe−Fe junction. The conductance histograms of pure Ni−Ni and Fe−Fe junctions have a typical main peak with a shoulder at the low conductance side (e.g., Figure 2c (I, III)). In both cases, this shape is ascribed to two or more populations of atomic contacts with different structures, and therefore somewhat different conductance is expected.[16,18,31] In view of Figure 3, the voltage pulse effectiveness seems to be related to the relative hardness of the two metals, although other properties such as surface energy, intermetallic bond strength, and the tendency for alloying may also play a role. For Au−Ni junctions, the applied pulse could not overcome the strong tendency of Ni wetting by Au, whereas for Fe−Ni electromigration of atoms from both electrodes was observed. In the "intermediate" case of Al−Pt junctions, a pulse that involves electron injection from the Pt electrode could introduce Pt atoms into the junction, though a pure Pt contact could not be obtained. The directionality of the induced atomic rearrangement can be nicely identified thanks to the two different metals used as electrodes. Thus, bimetallic break junctions can be an interesting system for the study of atomic-scale electromigration.

We now focus on bimetallic atomic contacts formed after applying a positive voltage pulse to the Al−Pt junctions. This procedure yielded the conductance histogram shown in Figure 3b (III). Figure 4a presents a length histogram of the last conductance plateaus measured during the elongation of Pt−Pt junctions. As mentioned before, a set of peaks in a length histogram indicates atomic-chain formation,[14,27−29,32−34] where the peaks reflect the relative probability for chains with a different number of atoms. Al−Al junctions, however, do not form atomic chains. Once a single Al atom contact is formed, it simply breaks when stretched without pulling atoms from the electrodes, though Al atomic dimers can be formed with a low probability. This is manifested by a shorter length histogram for Al−Al junctions (Figure 4b), with one main peak and a minor shoulder due to dimer formation. Al−Pt junctions produce length histograms similar to those of Al−Al junctions (Figure 4c). However, following the application of a positive voltage pulse with electrons injected from the Pt electrode, the length histogram changes considerably, as seen in Figure 4d. Here, the length distribution is clearly longer than expected for a single-atom contact. This behavior can be ascribed to the formation of atomic chains, despite the absence of well-separated peaks.[20] The lack of distinct peaks may indicate that the elongated chains are not exclusively made of Pt atoms. The histogram smearing can stem from atomic chains that contain

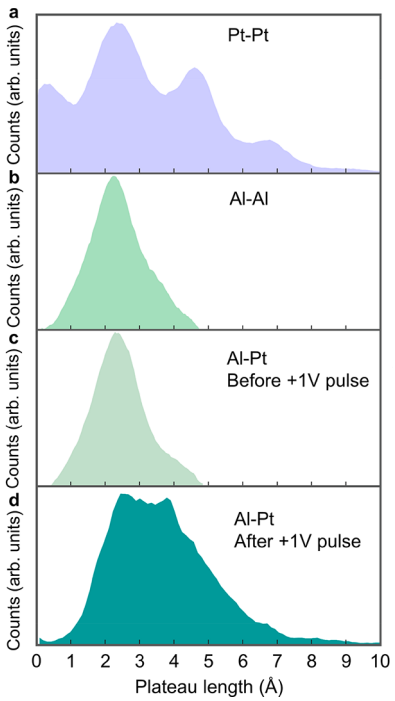

Figure 4. Length histograms of monometallic and bimetallic atomic-scale junctions. (a) Length histogram of Pt−Pt atomic-scale junctions. (b) Length histogram of Al−Al atomic-scale junctions. (c) Length histogram of Al−Pt atomic-scale junctions before the application of a voltage pulse. (d) Length histogram of Al−Pt atomic-scale junctions after the application of a positive voltage pulse (+1 V for 200 μs; electrons are injected from the Pt electrode to a 3 G_0 Al−Pt contact). Each histogram is based on 10,000 conductance vs interelectrode displacement traces taken during junction elongation at an applied voltage of 100 mV. Length histograms consider data in the conductance range of the main peak in the conductance histograms: (a) 1.0−2.5 G_0, (b) 0.3−1.3 G_0, (c) 0.3−1.3 G_0, and (d) 0.1−1.1 G_0 (see the mentioned conductance histograms in Figures 2 and 3).

different numbers of Pt and Al atoms and their permutations, leading to a large variety of chain lengths. Therefore, the data presented in Figure 4d and Figure 3b (III) suggest the formation of bimetallic atomic chains with lower conductance than that of Al−Al and Pt−Pt atomic junctions (see also calculations in Supporting Information, section 3). In Supporting Information, section 5, we suggest a chemical indication for the presence of Al atoms within the atomic chains. The indication is based on the conductance signature of Al atoms in elongated contacts that stems from the response of electronic states related to Al sp_z orbitals to interatomic stretching.[35−40] To date, the formation of suspended bimetallic atomic chains has been demonstrated only in atomic-scale constrictions in metal alloys, as reported for AuAg, AuCu, and PtIr alloys.[41−43] Here, we show that bimetallic atomic chains can be formed at the contact between two different metals (see Supporting Information, section 6).

To exemplify the potential of bimetallic junctions, we present an Fe−Ni spin-valve break junction. Although atomic and molecular spin-valve junctions have been demonstrated in break-junction setups (e.g., refs 44−46), these structures typically require nontrivial nanofabrication to promote magnetization switching in each electrode at a different applied magnetic field. Furthermore, careful design and challenging fabrication are required to minimize magnetostriction that leads to conductance variations due to changes in the

https://doi.org/10.1021/acs.nanolett.3c00508
Nano Lett. 2023, 23, 7775−7781

interelectrode distance when the magnetization changes. Here, we utilize the different coercive fields of Fe and Ni to flip the magnetization of each electrode separately in our Fe−Ni break junctions while collecting data on thousands of junctions. Figure 5 shows the most probable conductance of a single-

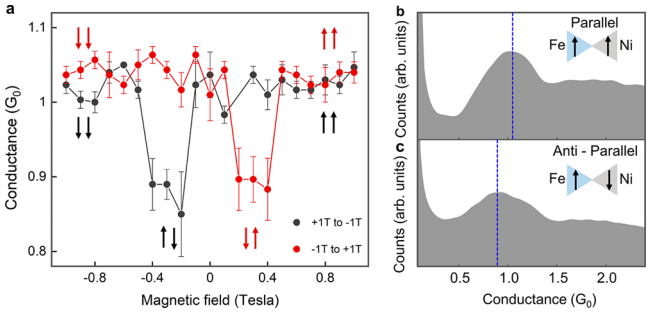

Figure 5. Mechanically controllable spin-valve junction. (a) Most probable conductance of Fe−Ni atomic junction as a function of applied magnetic fields perpendicular to the junction axis (T denotes Tesla). The data at each magnetic field are obtained from at least 5 consecutive conductance histograms. Each histogram is based on 10,000 conductance traces measured during junction elongation, at a bias voltage of 100 mV. The error bars provide the standard deviation of the averaged data. (b, c) Conductance histograms taken at magnetic fields of −1 T (b) and −0.2 T (c), yielding a relative high and low most probable conductance (blue dashed lines), ascribed to parallel and antiparallel magnetization as illustrated in the insets, respectively.

atom contact in Fe−Ni junctions as a function of magnetic fields perpendicular to the junction axis. At each magnetic field, several conductance histograms were taken consequentially, and the average conductance value of the main peak in these histograms is presented in Figure 5a. Examples of conductance histograms taken under different fields for parallel and antiparallel electrode magnetizations are seen in Figure 5b,c (see also the Supporting Information, section 7). The conductance is high for a parallel magnetization, and it is lower for an antiparallel magnetization. Between 0.2 and 0.4 T (or −0.2 and −0.4 T), where T denotes Tesla, the field is high enough to flip the magnetization in the Ni electrode (Ni has a lower coercive field than Fe), while the magnetization direction of the Fe electrode is preserved. However, above this field range, the magnetization of the Fe electrode flips as well, yielding a parallel magnetization. The obtained magnetoresistance (MR) of 7.6 ± 0.7% is typical for atomic spin valves of ferromagnetic metals[44] (MR = $(G_P - G_{AP})/(G_P + G_{AP})$, where G_P and G_{AP} are the conductance for parallel and antiparallel configurations, respectively). This bimetallic structure can therefore serve as a platform for molecular-junction spin valves. Using bimetallic break junctions as a spin valve has the following advantages: (i) complicated nanofabrication is not required; (ii) avoidance of magnetostriction artifacts, since conductance histograms are collected at fixed magnetic fields and magnetizations; (iii) magnetoresistance of thousands of junctions can be collected in a short time; and (iv) high mechanical stability is preserved. Thus, a spin-valve break junction can be used as a convenient setup for the study of spin transport and magnetism in atomic or molecular junctions.

The rich structures of atomic-scale contacts formed when two different metals are repeatedly pressed can provide a versatile platform for scientific research. For example, bimetallic junctions can serve as a natural testbed for the study of alloys with reduced dimensions, bimetallic atomic interfaces, electromigration at the atomic scale, and proximity effects related to atomic structures near superconducting or ferromagnetic electrodes. The compositions and geometries of bimetallic atomic contacts are also attractive for the study of spin, charge, and heat transport at the atomic scale. Furthermore, the introduction of molecules to bimetallic junctions can merge the structural advantages of these junctions and that of molecules to gain a wealth of new properties and functionalities.

■ ASSOCIATED CONTENT

Supporting Information

The Supporting Information is available free of charge at https://pubs.acs.org/doi/10.1021/acs.nanolett.3c00508.

Experimental details, control experiments, table of metal hardness, recognition of Al atoms in atomic-chains formed in Al−Pt junctions, Al−Pt junction response to repeated deformation cycles after pulse application, density functional theory and transport calculations, including technical calculation details (PDF)

■ AUTHOR INFORMATION

Corresponding Author

Oren Tal − *Department of Chemical and Biological Physics, Weizmann Institute of Science, Rehovot 7610001, Israel;* orcid.org/0000-0002-3625-1982

Authors

Anil Kumar Singh − *Department of Chemical and Biological Physics, Weizmann Institute of Science, Rehovot 7610001, Israel*

Sudipto Chakrabarti − *Department of Chemical and Biological Physics, Weizmann Institute of Science, Rehovot 7610001, Israel; Surface Physics and Material Science Division, Saha Institute of Nuclear Physics, Kolkata 700064, India*

Ayelet Vilan − *Department of Chemical and Biological Physics, Weizmann Institute of Science, Rehovot 7610001, Israel;* orcid.org/0000-0001-5126-9315

Alexander Smogunov − *SPEC, CEA, CNRS, Université Paris-Saclay, CEA Saclay, Gif sur Yvette 91191, France*

Complete contact information is available at: https://pubs.acs.org/10.1021/acs.nanolett.3c00508

Notes

The authors declare no competing financial interest.

■ ACKNOWLEDGMENTS

O.T. appreciates the support of the Harold Perlman family and acknowledges funding by a research grant from Dana and Yossie Hollander, the Ministry of Science and Technology of Israel (Grant No. 3-16244), and the European Research Council, Horizon 2020 (Grant No. 864008). The calculations were performed using HPC resources from GENCI (project AD010910407R1)

■ REFERENCES

(1) Agraıt, N.; Yeyati, A. L.; van Ruitenbeek, J. M. Quantum properties of atomic-sized conductors. *Phys. Rep.* **2003**, *377*, 81−279.

(2) Cuevas, J. C.; Scheer, E. *Molecular Electronics: An Introduction to Theory and Experiment;* World Scientific Publishing, 2017.
(3) Scott, G. D.; Natelson, D. Kondo Resonances in Molecular Devices. *ACS Nano* **2010**, *4* (7), 3560−3579.
(4) Aradhya, S. V.; Venkataraman, L. Single-molecule junctions beyond electronic transport. *Nat. Nano.* **2013**, *8*, 399−410.
(5) Gehring, P.; Thijssen, J. M.; van der Zant, H. S. J. Single-Molecule Quantum-Transport Phenomena in Break Junctions. *Nat. Rev. Phys.* **2019**, *1* (6), 381−396.
(6) Evers, F.; Korytár, R.; Tewari, S.; van Ruitenbeek, J. M. Advances and Challenges in Single-Molecule Electron Transport. *Rev. Mod. Phys.* **2020**, *92* (3), 035001.
(7) Scheer, E.; Agrait, N.; Cuevas, J. C.; Yeyati, A. L.; Ludoph, B.; Martin-Rodero, A.; Bollinger, G. R.; van Ruitenbeek, J. M.; Urbina, C. The signature of chemical valence in the electrical conduction through a single-atom contact. *Nature* **1998**, *394*, 154−157.
(8) Scheer, E.; Belzig, W.; Naveh, Y.; Devoret, M. H.; Esteve, D.; Urbina, C. Proximity Effect and Multiple Andreev Reflections in Gold Atomic Contacts. *Phys. Rev. Lett.* **2001**, *86*, 284−287.
(9) Landman, U.; Luedtke, W. D.; Burnham, N. A.; Colton, R. J. Atomistic mechanisms and dynamics of adhesion, nanoindentation, and fracture. *Science* **1990**, *248*, 454−461.
(10) Landman, U.; Luedtke, W. D.; Ringer, E. M. Atomistic mechanisms of adhesive contact formation and interfacial processes. *Wear* **1992**, *153*, 3−30.
(11) Fian, A.; Ernst, C.; Leisch, M. Combined atom probe and STM study of tip−substrate interactions Fresenius. *J. Anal. Chem.* **1999**, *365*, 38−42.
(12) Fian, A.; Leisch, M. Study on tip−substrate interactions by STM and APFIM. *Ultramicroscopy* **2003**, *95*, 189−197.
(13) Rubio, G.; Agraït, N.; Vieira, S. Atomic-sized metallic contacts: mechanical properties and electronic transport Phys. *Rev. Lett.* **1996**, *76*, 2302−2305.
(14) Yanson, A. I.; Bollinger, G. R.; Van den Brom, H. E.; Agrait, N.; Van Ruitenbeek, J. M. Formation and manipulation of a metallic wire of single gold atoms. *Nature* **1998**, *395*, 783−785.
(15) Dreher, M.; Pauly, F.; Heurich, J.; Cuevas, J. C.; Scheer, E.; Nielaba, P. Structure and Conductance Histogram of Atomic-Sized Au Contacts. *Phys. Rev. B* **2005**, *72*, 075435.
(16) Calvo, M. R.; Caturla, M. J.; Jacob, D.; Untiedt, C.; Palacios, J. J. Mechanical, electrical and magnetic properties of Ni nanocontacts. *IEEE Trans. Nanotechnol.* **2008**, *7*, 165−168.
(17) Calvo, M. R.; Fernández-Rossier, J.; Palacios, J. J.; Jacob, D.; Natelson, D.; Untiedt, C. The Kondo effect in ferromagnetic atomic contacts. *Nature* **2009**, *458*, 1150−1153.
(18) Dednam, W.; Sabater, C.; Tal, O.; Palacios, J. J.; Botha, A. E.; Caturla, M.J. Refined electron-spin transport model for single-element ferromagnetic systems: Application to nickel nanocontacts. *Phys. Rev. B* **2020**, *102*, 245415.
(19) Untiedt, C.; Dekker, D. M. T.; Djukic, D.; van Ruitenbeek, J. M. Absence of magnetically induced fractional quantization in atomic contacts. *Phys. Rev. B* **2004**, *69* (8), 081401.
(20) Vardimon, R.; Klionsky, M.; Tal, O. Indication of complete spin filtering in atomic-scale nickel oxide. *Nano Lett.* **2015**, *15*, 3894−3898.
(21) van den Brom, H. E.; van Ruitenbeek, J. M. Quantum Suppression of Shot Noise in Atom-Size Metallic Contacts. *Phys. Rev. Lett.* **1999**, *82*, 1526−1529.
(22) Jacob, D.; Fernández-Rossier, J.; Palacios, J. Magnetic and orbital blocking in Ni nanocontacts. *Phys. Rev. B* **2005**, *71* (22), 220403.
(23) Häfner, M.; Viljas, J. K.; Frustaglia, D.; Pauly, F.; Dreher, M.; Nielaba, P.; Cuevas, J. C. Theoretical study of the conductance of ferromagnetic atomic-sized contacts. *Phys. Rev. B* **2008**, *77* (10), 104409.
(24) Vardimon, R.; Matt, M.; Nielaba, P.; Cuevas, J. C.; Tal, O. Orbital origin of the electrical conduction in ferromagnetic atomic-size contacts: insights from shot noise measurements and theoretical simulations. *Phys. Rev. B* **2016**, *93*, 085439.
(25) Samsonov, G. V. *Handbook of the Physicochemical Properties of the Elements;* Springer, 2012.
(26) Egle, S.; Bacca, C.; Pernau, H. F.; Huefner, M.; Hinzke, D.; Nowak, U.; Scheer, E. Magnetoresistance of atomic-size contacts realized with mechanically controllable break junctions. *Phys. Rev. B* **2010**, *81*, 134402.
(27) Smit, R. H. M.; Untiedt, C.; Yanson, A. I.; van Ruitenbeek, J. M. Common origin for surface reconstruction and the formation of chains of metal atoms. *Phys. Rev. Lett.* **2001**, *87*, 266102.
(28) Smit, R. H. M.; Untiedt, C.; Rubio-Bollinger, G.; Segers, R. C.; van Ruitenbeek, J. M. Observation of a Parity Oscillation in the Conductance of Atomic Wires. *Phys. Rev. Lett.* **2003**, *91*, 076805.
(29) Vardimon, R.; Yelin, T.; Klionsky, M.; Sarkar, S.; Biller, A.; Kronik, L.; Tal, O. Probing the Orbital Origin of Conductance Oscillations in Atomic Chains. *Nano Lett.* **2014**, *14* (6), 2988−2993.
(30) Thijssen, W. H. A.; Marjenburgh, D.; Bremmer, R. H.; van Ruitenbeek, J. M. Oxygen-Enhanced Atomic Chain Formation. *Phys. Rev. Lett.* **2006**, *96*, 026806.
(31) Dednam, W.; Sabater, C.; Calvo, M. R.; Untiedt, C.; Palacios, J. J.; Botha, A. E.; Caturla, M. J. Directional bonding explains the high conductance of atomic contacts in bcc metals. *Phys. Rev. B* **2020**, *101*, 165417.
(32) García-Suárez, V. M.; Rocha, A. R.; Bailey, S. W.; Lambert, C. J.; Sanvito, S.; Ferrer, J. Conductance Oscillations in Zigzag Platinum Chains. *Phys. Rev. Lett.* **2005**, *95*, 256804.
(33) Shiota, T.; Mares, A. I.; Valkering, A. M. C.; Oosterkamp, T. H.; van Ruitenbeek, J. M. Mechanical Properties of Pt Monatomic Chains. *Phys. Rev. B* **2008**, *77*, 125411.
(34) Chakrabarti, S.; Vilan, A.; Deutch, G.; Oz, A.; Hod, O.; Peralta, J. E.; Tal, O. Magnetic control over the fundamental structure of atomic wires. *Nature Commun.* **2022**, *13*, 1−2.
(35) Krans, J. M.; Muller, C. J.; Yanson, I. K.; Govaert, T. C. M.; Hesper, R.; van Ruitenbeek, J. M. One-atom point contacts. *Phys. Rev. B* **1993**, *48*, 14721−14724.
(36) Scheer, E.; Joyez, P.; Estève, D.; Urbina, C.; Devoret, M. H. Conduction Channel Transmissions of Atomic-Size Aluminum Contacts. *Phys. Rev. Lett.* **1997**, *78*, 3535−3538.
(37) Cuevas, C.; Yeyati, A. L.; Martin-Rodero, A. Microscopic Origin of Conducting Channels in Metallic Atomic-Size Contacts. *Phys. Rev. Lett.* **1998**, *80*, 1066.
(38) Cuevas, J. C.; Levy Yeyati, A.; Martín-Rodero, A.; Rubio Bollinger, G.; Untiedt, C.; Agraït, N. Evolution of Conducting Channels in Metallic Atomic Contacts under Elastic Deformation. *Phys. Rev. Lett.* **1998**, *81*, 2990.
(39) Jelínek, P.; Pérez, R.; Ortega, J.; Flores, F. First-principles simulations of the stretching and final breaking of Al nanowires: Mechanical properties and electrical conductance. *Phys. Rev. B* **2003**, *68*, 085403.
(40) Vardimon, R.; Klionsky, M.; Tal, O. Experimental determination of conduction channels in atomic-scale conductors based on shot noise measurements. *Phys. Rev. B* **2013**, *88*, 161404.
(41) Bettini, J.; Sato, F.; Coura, P. Z.; Dantas, S. O.; Galvao, D. S.; Ugarte, D. Experimental realization of suspended atomic chains composed of different atomic species. *Nat. Nanotechnol.* **2006**, *1*, 182.
(42) Lagos, M. J.; Autreto, P. A. S.; Bettini, J.; Sato, F.; Dantas, S. O.; Galvao, D. S.; Ugarte, D. Surface Effects on the Mechanical Elongation of AuCu Nanowires: De-Alloying and the Formation of Mixed Suspended Atomic Chains. *J. Appl. Phys.* **2015**, *117*, 094301.
(43) Ochiai, Y.; Obi, T.; Tsuruoka, Y.; Kizuka, T. Element Mapping in Single-Atom-Width Platinum−Iridium Wires. *Nano Lett.* **2020**, *20*, 2169−2174.
(44) Bolotin, K. I.; Kuemmeth, F.; Pasupathy, A. N.; Ralph, D. C. From ballistic transport to tunneling in electromigrated ferromagnetic breakjunctions. *Nano Lett.* **2006**, *6*, 123−127.
(45) Yoshida, K.; Hamada, I.; Sakata, S.; Umeno, A.; Tsukada, M.; Hirakawa, K. Gate-Tunable Large Negative Tunnel Magnetoresistance in Ni-C_{60}-Ni Single Molecule Transistors. *Nano Lett.* **2013**, *13* (2), 481−485.

https://doi.org/10.1021/acs.nanolett.3c00508
Nano Lett. 2023, 23, 7775−7781

(46) Scott, G. D.; Hu, T. C. Gate-controlled Kondo effect in a single-molecule transistor with elliptical ferromagnetic leads. *Phys. Rev. B* **2017**, *96*, 144416.

https://doi.org/10.1021/acs.nanolett.3c00508
Nano Lett. 2023, 23, 7775−7781

Supporting Information

Electrically-controlled bimetallic junctions for atomic-scale electronics

Anil Kumar Singh[1], Sudipto Chakrabarti[1,2], Ayelet Vilan[1], Alexander Smogunov[3], and Oren Tal[1,*]

[1]*Department of Chemical and Biological Physics, Weizmann Institute of Science, Rehovot 7610001, Israel*

[2]*Surface Physics and Material Science Division, Saha Institute of Nuclear Physics, Kolkata 700064, India*

[3]*SPEC, CEA, CNRS, Université Paris-Saclay, CEA Saclay, Gif sur Yvette 91191, France*

* Corresponding author

Content:

Section 1: Experimental details

Section 2: Control Experiments with monometallic junctions

Section 3: Density functional theory and transport calculations

Section 4: Supplementary table of metal hardness

Section 5: Recognition of Al atoms in atomic chains formed in Al-Pt junctions

Section 6: Al-Pt junction response to repeated deformation cycles after pulse application

Section 7: Spin-valve experiments

Section 1: Experimental details

We use a mechanical controllable break-junction set-up[S1] to fabricate the study bimetallic atomic scale structures (Figure 1a, main text). The break junction samples are composed of two wires (supplier: Alfa Aesar, diameter: 0.1 mm, length 12 mm) each made of a different metal, with the following purities: 99.994% (Ni), 99.998% (Au), 99.997% (Pt) 99.999% (Al), and 99.998% (Fe). First, the two wires are cut to have a sharp tip at one end. Then, as illustrated in Figure 1, in the main text, a flexible substrate is temporarily bent in the middle (1-mm-thick phosphor-bronze plate covered by 100 μm insulating Kapton film), and the wires are attached to the substrate such that their tips are in contact. Finally, the bent substrate is relaxed, such that the flexible substrate is straitened, and the two metal tips are squeezed into each other to form a larger contact between the two tips. Samples, with the same metal electrodes are formed by attaching a single wire (24 mm in length) with a notch (partial cut) at its center to the flexible substrate.

The sample is placed in a vacuum chamber that is pumped and cooled to ~4.2K. With the aid of a three-point bending mechanism including a piezoelectric element (PI P-882 PICMA) connected to a Piezomechanik SVR 150/1 piezo driver, which is driven by a 24-bit NI-PCI4461 or a NI-PXI4461 data acquisition (DAQ) card, the substrate is bent in cryogenic vacuum conditions to either break the contact between the wires for bimetallic junctions or break the wire at the notch for monometallic junctions. Since the three-points bending mechanism translates the movement of the piezoelectric element to more than two orders of magnitude attenuated interelectrode displacement, the distance between the electrode apices can be controlled in sub-Ångstrom resolution. Stretching the contact/notch reduces the number of atoms in the cross section of the constriction down to a single atom, where further stretching leads to junction rapture into two atomically sharp apices. To promote the formation of new structures at the contact and collect information on the span of possible formed structures at the contact, the junction can be repeatedly broken and reformed (typically up to conductance of 70 G_0) at a rate of 20–40 Hz, while the conductance of the junction is measured simultaneously via the two wire segments that serve as electrodes.

To measure conductance, the junction is biased with a d.c. voltage provided by the NI-PCI4461 or NI-PXI4461 DAQ card. The presented measurements are performed at a bias voltage of 100 mV (1,000 mV is applied by the DAQ card, via a 1/10 voltage divider to improve the signal to noise

ratio). The resulting current from the junction is amplified by a current amplifier (Femto amplifier DLPCA 200) and recorded by the DAQ card. To extract the conductance, the obtained current values are divided by the applied voltage values. The interelectrode displacement is found by the exponential dependence of tunneling currents on the separation between the electrodes[S2].

Histogram formation: Conductance histograms were formed using 200 bins with a bin width of 0.02 G_0 (linear histograms). Length histogram were constructed using dedicated MatLab code. In short, the code counts the number (n_t) of readings (G_i), within a specific conductance window ($[G_{min} \quad G_{max}]$) for each pull trace: $n_t = \sum G_{min} \leq G_i \leq G_{max}$; the net length per trace (L_t) is defined as: $L_t = \kappa \cdot \Delta V_p \cdot (n_t - 1)$, where κ is the break-junction spring constant deduced from the tunneling-decay slope and ΔV_p is the increment in piezo-voltage. Finally, a histogram is made by MatLab standard function: *histcounts.m* using as input the ~10,000-long array of L_t values deduced for the entire dataset (no selection).

Application of a voltage pulse: Figures 2aII, 2bII, and 2cII in the main text present typical conductance histograms of the relevant bimetallic junctions before the application of a voltage pulse. Subsequently, we formed a junction with 3 G_0 conductance and applied a single +1 V or a -1 V voltage pulse for 200 μs. Following the single pulse application, we recorded another conductance histogram, such as Figures 2aI or 2aIII, 2bI or 2bIII, and 2cI or 2cIII. To restore the initial conductance histograms, we repeatedly broke and reformed the junction, where during the formation we reached ~70 G_0 to promote junction deformation. This process was applied for 35,000 cycles for all three bimetallic junctions after a pulse procedure, even when no apparent change in the conductance histogram was seen (e.g., in the case of Au-Ni). Following the described procedure, and after ensuring a successful reconstruction of a conductance histogram identical to the initial one, another pulse was given and the procedure was repeated.

Section 2: Control Experiments with monometallic junctions

Out of the monometallic junctions based on Au, Ni, Al, Pt, and Fe that are used in this work, the shape of the conductance histograms of Ni and Pt junctions are the most sensitive to contaminations within the junction. Therefore, we selected these two metals as testbeds in the following experiments. We fabricated Ni-Ni and Pt-Pt break junction samples based on two sharp electrodes prepared in ambient conditions using an identical procedure to the one used for the bimetallic break junctions (as described in Section 1). Figure S1 shows that the conductance histograms of these junctions are identical to the ones of Ni-Ni and Pt-Pt break junctions fabricated using a single wire (made of Ni or Pt, respectively) that was broken only after cryogenic conditions were achieved. Interestingly, the presented histograms in Figures S1a,b were recorded after 1,000 initial repeated breaking and formation cycles, indicating that the removal of possible contaminations does not require considerable efforts.

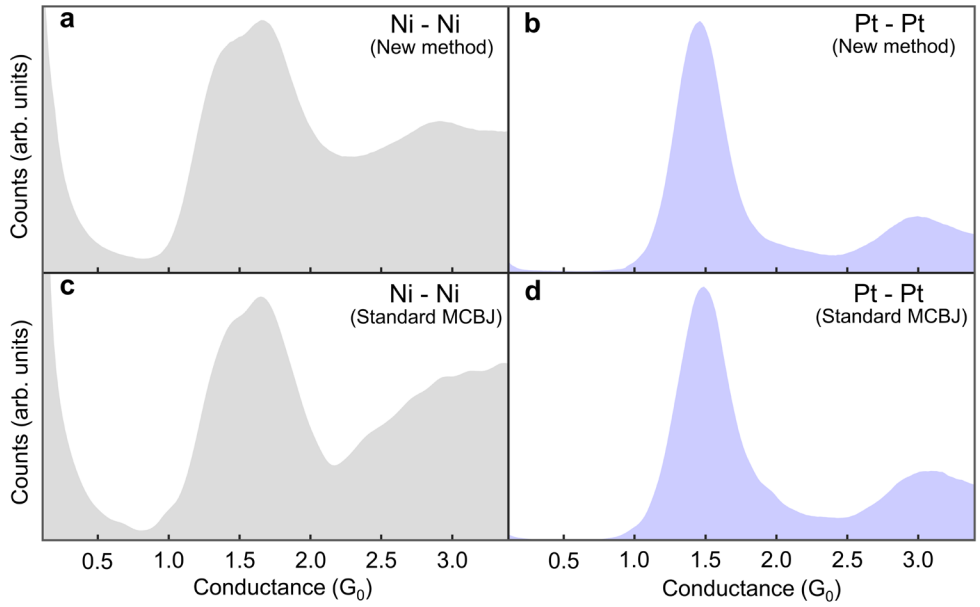

Figure S1: (a,b) Conductance histograms of Ni-Ni (a) and Pt-Pt (b) atomic junctions prepared using the new MCBJ preparation method described in Section 1. (c,d) Conductance histograms of Ni-Ni (b) and Pt-Pt (c) atomic junctions prepared using the standard MCBJ preparation method described in Section 1. The peaks indicate the most probable conductance of the atomic scale contacts during their elongation. The measurements were done at 100 mV applied voltage, and the histograms are composed of 10,000 conductance traces each.

Section 3: Density functional theory and transport calculations

Figure S2 presents the calculated transmission for junctions with different metallic compositions, where the transmission at the Fermi energy provides the conductance in units of G_0. The associated projected density of states (s and p for Al, s and d for Pt, Ni and Fe) on the central apex atoms are presented we well.

Bellow, we list relevant information about the calculations:

1. To overcome the technical limitations involved with calculations of contacts between two different metal electrodes, we used the same metal for the two electrodes, with different metal atoms at the contact, as illustrated in Figure S2, top insets. This is done under the assumption that the transmission properties of the atomic junctions are dominated by the atoms at the contact vicinity.

2. For Ni-Ni and Ni-Fe junctions, we present in Figure S2d the spin resolved PDOS. However, the presented transmission in Figure S2b provides the sum of spin up and down contributions, since we are interested in comparing the calculations to the measured total (spin up and down) conductance.

3. Pt-Pt and Fe-Fe atomic junctions have a higher measured conductance than Al-Al and Ni-Ni junctions, respectively. Here, we do not present calculations for these junctions. Instead, we focus on a comparative analysis between the transmission of the less conducting Al-Al and Ni-Ni counterpart junctions with respect to their relevant bimetallic systems Al-Pt and Ni-Fe, respectively.

4. When introducing Pt atoms to the Al hosting structure to form an abrupt Al-Pt atomic contact, the two atoms tend to mix at their back multi-atomic interface (Figure S2a, red frame Inset, inside the right electrode apex) after structural relaxation. This is in contrast to the case of an abrupt Ni-Fe contact, where the initially well-separated Fe and Ni atomic sub-systems are kept separated after structural relaxation (Figure S2b red frame Inset, inside the right electrode apex).

5. When considering an alloy contact at the junction constriction, we locally form an alloy made of a similar number of atoms of each metal as a representative composition. More elaborated calculations for different alloy compositions in the junctions are beyond the scope of this Letter.

Focusing on the calculations outcome, the calculated ~0.9 G_0 transmission for an Al-Al atomic junction (Figure S2a; black) at the Fermi energy is very close to the measured conductance for Al-Al atomic junctions, as obtained by conductance histograms (e.g., Figure 1bI, main peak around 0.8 G_0). Conductance histograms obtained for Ni-Ni junctions reveal two main most probable conductance values at ~1.6 G_0 and sometimes also at ~ 1.2 G_0 (e.g., Figure 2cIII), ascribed to two dominant stable configurations (Refs.16-20 in the main text). Here, the calculated transmission (Figure S2b; black) at the Fermi energy agrees well with the measured ~1.6 G_0 conductance.

Figure S2a shows that an abrupt contact between Al and Pt (red) has a higher transmission than the Al-Al junction (black). Interestingly, even an alloy contact with a short chain shows a higher transmission compared to the Al-Al atomic junction (blue). Note that we first produced a single atom contact alloy but following relaxation a short atomic chain was formed, indicating that such a chain is energetically favorable. In contrast to the mentioned cases, a lower calculated transmission is clearly observed for an Al-Pt alloy at the contact with a longer atomic chain that adapt (to some extent) a zigzag configuration. This structure was formed by increasing the interelectrode separation in the former structure, following by relaxation. This process yielded the longer chain, again showing the preference for Al-Pt bimetallic chain formation. Note that the elongation of the chain leads to PDOS reduction on the Pt central atom, which we associate with the observed reduction in transmission. To summarize, an abrupt Al-Pt atomic contact cannot explain our experimental observations, and the same applies to the considered alloy Al-Pt junction. Conversely, an alloy junction with a longer atomic chain does show a clear reduction in transmission with a value at the Fermi energy (~ 0.64) closer to the observed conductance after the application of a positive voltage pulse (Figure 3bIII, main peak centered at ~ 0.45 G_0 with a tail towards a higher conductance). This is consistent with experimental indications for the elongation of bimetallic Al-Pt atomic chains following the application of a +1V pulse (before pulse: Figure 4c; after pulse: Figure 4d), alongside with a reduction in conductance (before pulse: Figure 3bII; after pulse: Figure 3bIII).

Figure S2b shows that a junction with an abrupt bimetallic Fe-Ni contact, and a Fe/Ni alloy contact have a lower transmission at the Fermi energy than that of a Ni-Ni atomic junction. For an abrupt Ni-Fe junction the transmission has a dip around the Fermi energy. As a result, the conductance is close to 1 G_0. The PDOS analysis in Figure S2d allows attributing this dip to a significant depletion

of spin down d-states at the Fermi energy on the Ni apex atom, driven by hybridization between the Ni and Fe apex atoms. A similar effect is also seen for the alloy Ni-Fe junction, even within a wider energy window around the Fermi energy. To summarize, in view of the calculations the lower measured conductance for Ni-Fe junctions in comparison to Ni-Ni junctions can be ascribed to the formation of either an abrupt bimetallic contact or an alloy at the junction's constriction.

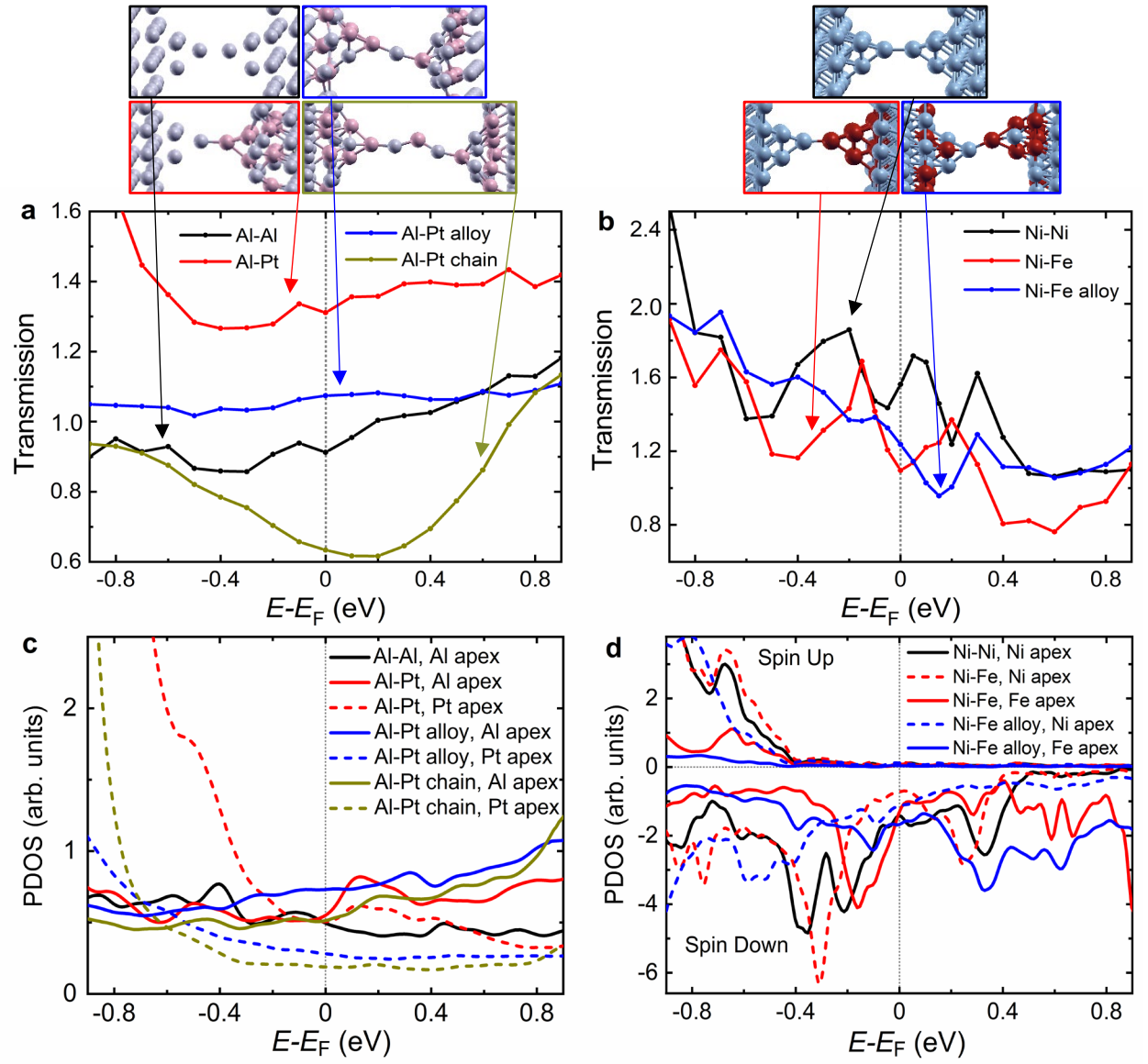

Figure S2: Calculated transmission and projected density of states (PDOS) for atomic junctions. (a) Transmission of Al-Al and different Al-Pt atomic junctions. (b) Transmission of Ni-Ni and different Ni-Fe atomic junctions. (c) PDOS of Al-Al and different Al-Pt atomic junctions. (d) Spin resolved PDOS of Ni-Ni and different Ni-Fe atomic junctions. In all cases the projection is done on the most central atoms.

Technical details:

In order to interpret the experimental results, we performed density functional theory (DFT) calculations using Quantum-ESPRESSO (QE)[S3] package with Perdew-Burke-Ernzerhof (PBE)[S4] parametrization for exchange-correlation functionals. We concentrated on several structures of Al,Pt and Ni,Fe based junctions. The atomic junctions were simulated by supercells consisting of three (left) and four (right) Al or Ni atomic layers in the (111) crystallographic orientation connected by two 4-atoms pyramids as shown in Figure S2. A (4x4) in-plane periodicity (16 atoms per layer) was employed to avoid artificial interactions between junctions. The energy cut-offs of 30 and 300 Ry were used for the wave functions and charge density expansions over plane waves, while electron-ions interactions were described by ultra-soft pseudopotentials. A (4x4x1) k-mesh was adopted with a smearing parameter of 0.01 Ry in order to integrate over the Brillouin zone.

In order to simulate bi-metallic junctions, the composition of the two pyramids and the six closest atoms of the surface layers (making up the extended pyramids of 10 atoms each) was modified. For the case of abrupt junctions, the Al or Ni atoms of only the right pyramid were completely replaced by Pt or Fe, respectively, while for alloy junctions the composition of both extended pyramids was partially modified in a random way. Note that such geometries rely on the assumption that principal scattering processes occur in the narrowest part of the system - at the pyramid-pyramid junction - rather than at the pyramid/electrode interfaces, which seems to be reasonable due to the significantly larger atomic coordination of the latter. These initial structures were subsequently optimized, where the atoms of only two surface layers and the pyramids were allowed to relax until the atomic forces were smaller than 10-4 Ry/bohr.

The (spin-polarized) transport calculations were carried out using PWcond[S5] code (included in QE), the supercell described above was augmented by 3 atomic layers on each side and then attached to two semi-infinite electrodes. The total transmission function was calculated by averaging over a (6x6) in-plane mesh of k-points.

Section 4: Supplementary table of metal hardness

Metals	Ni	Fe	Pt	Al	Au
Mohs scale	4.0	4.0	3.5	2.75	2.5
Vickers hardness (MPa)	638	608	400-549	160-350	188-216

Table S1: Hardness of metals at room temperature, based on Ref. S6.

Section 5: Recognition of Al atoms in atomic chains formed in Al-Pt junctions

While the elongation of Al-Pt atomic junctions does not form atomic chains, it is shown in the main text that following the application of a +1V pulse for 200 μsec (electrons are injected from the Pt electrode), suspended atomic chains can be elongated between the electrode apices during the stretching process of Al-Pt junctions. The lack of a clear set of peaks in the length histogram presented in Figure 4d in the main text indicates structural richness beyond that of atomic chains that contain a single type of atoms. Thus, the presence of Al atoms in the atomic chains can be expected. Here, we provide a clear indication for the presence of Al atoms within the formed atomic chains.

Stretching Al-Al as well as Pt-Pt atomic contacts leads to an increase in the conductance due to an increase in the local density of states at the Fermi energy as a result of changes in the overlap of atomic orbitals[S7-S10]. However, the increase in the conductance of stretched Al atomic scale contacts has a very pronounced and peculiar convex shape, as can be seen in Figure S3a[S7,S11-S13]. For Pt atomic scale contacts, the exact shape of the conductance increase during stretching is less defined, though it has mostly a concave shape as observed in Figure S3b[S2,S10]. Figures S3c-e present typical traces of conductance vs. displacement for Al-Pt that were measured after the application of a +1V pulse. The detection of the mentioned typical convex features at different locations along the traces indicates the presence of Al atoms in the elongated atomic chain.

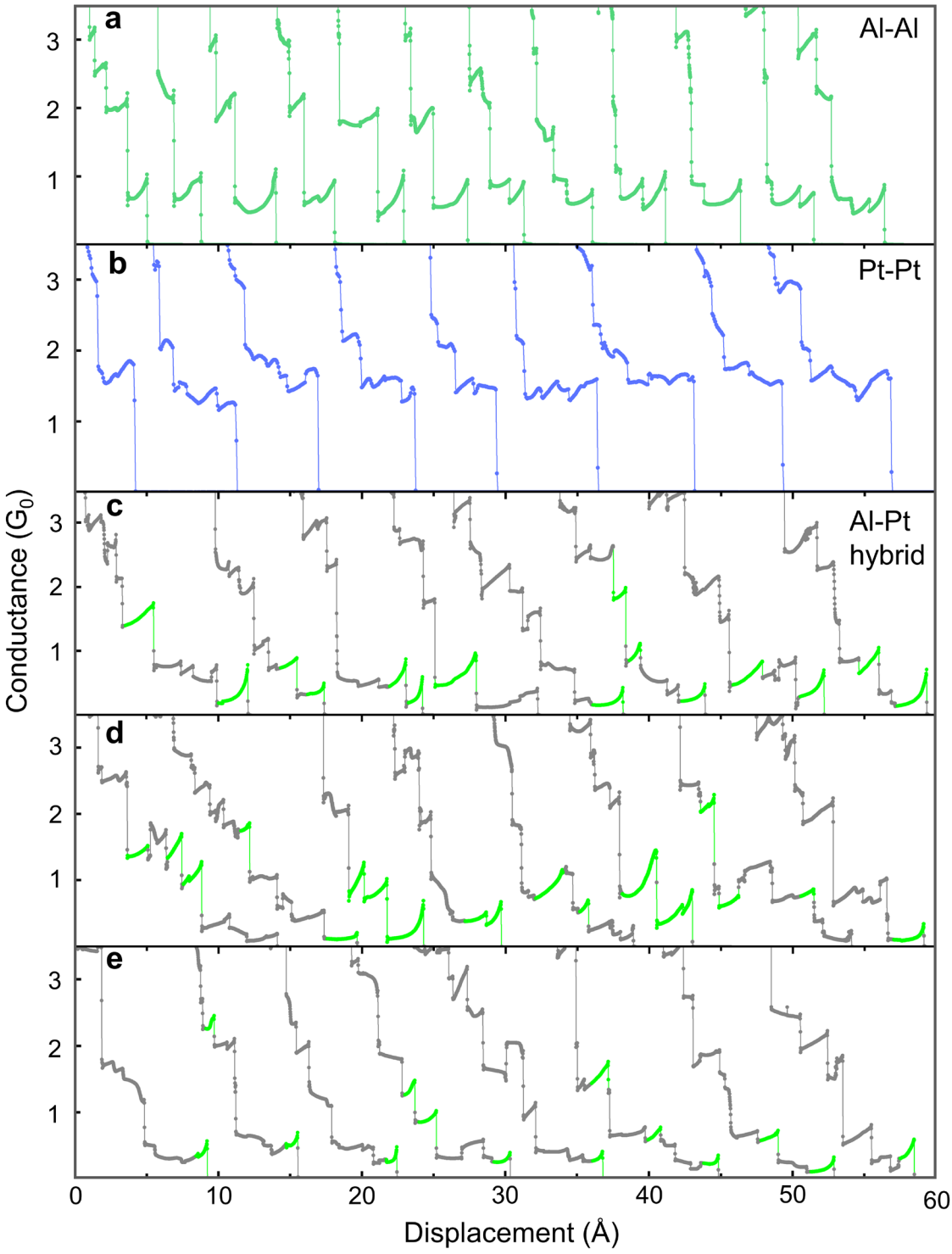

Figure S3: Conductance versus displacement of different junctions. Examples for traces of conductance versus interelectrode displacement for Al-Al junctions (a), Pt-Pt junctions (b), and Al-Pt junctions after the application of a +1V pulse (c-e). Convex features that indicate the presence of Al atoms are marked in (c-e) in green. The measurements were done at an applied voltage of 100 mV.

Section 6: Al-Pt junction response to repeated deformation cycles after pulse application

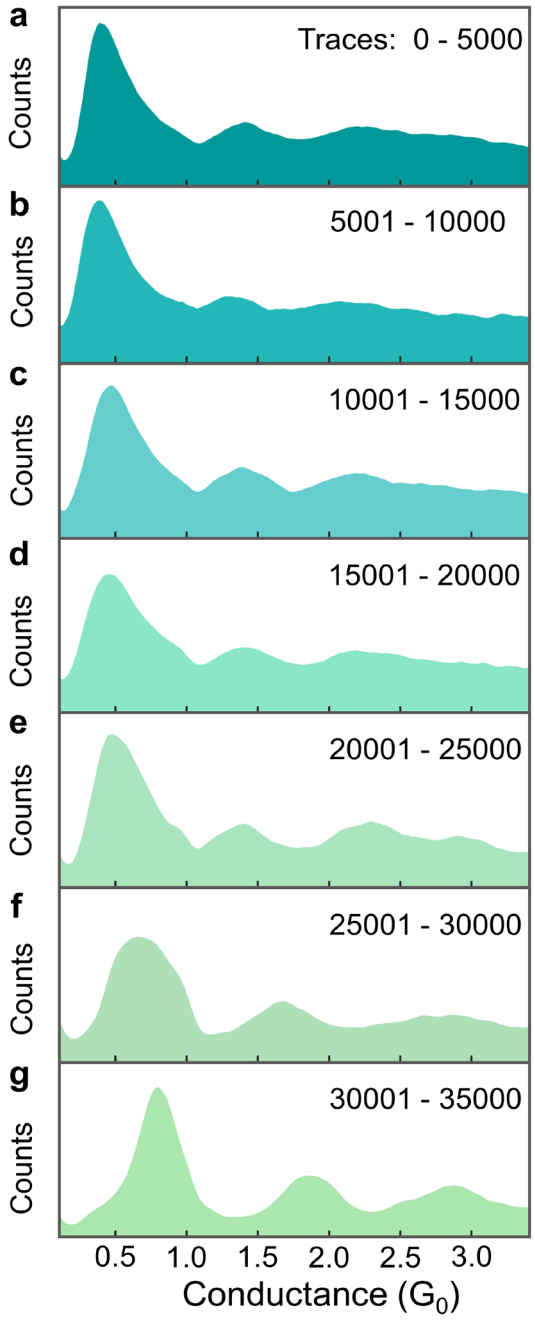

Figure S4: Evolution of conductance histograms of Al-Pt atomic-scale junctions after the application of a positive voltage pulse. The conductance histogram is gradually changing. For example, the main peak at ~0.4 G_0 is shifted to ~0.8 G_0. To achieve a detectable change over 35,000 traces, the two electrodes are squeezed repeatedly to have a contact of ~25 G_0. The total time elapsed between traces number 1 and 35,000 is about 50 min. Each conductance histogram is based on 5,000 conductance versus inter-electrode displacement traces, taken during junction elongation at an applied voltage of 100 mV.

Following an applied voltage pulse to the Al-Pt bimetallic junction with electrons injected from the Pt electrode, a bimetallic structure is formed in the junction. However, in response to repeated mechanical manipulation with high enough squeezing amplitude (tens of G_0), the contact is changing as a function of squeezing events to eventually yield the characteristics of Al-Al junctions, as seen in Figure S4. To preserve an Al-Pt bimetallic contact for a practical timeframe of several hours, one needs to limit the squeezing amplitude of the contacts to a few G_0.

Section 7: Fe-Ni spin valve experiments

Before the application of magnetic fields, the Fe-Ni junctions were repeatedly broken and reformed for thousands of times until stable histograms at 100 mV were obtained as a function of time. Next, a constant magnetic field of +3 Tesla was applied perpendicular to the junction's axis and the junction was broken and reformed for several thousands of times. This procedure promotes initial alignment of magnetization. In the following step, a constant magnetic field of +1 Tesla was applied perpendicular to the junction's axis and several consecutive conductance histograms of 5,000 traces each were collected (e.g., Figure S5a). The magnetic field was chosen to be perpendicular to the junction since in former experiments, where magnetic fields were applied along the junction's axis, we could observe magneto-conductance behavior that can be ascribed to a non-collinear magnetization in the two electrodes due to an easy axis of magnetization perpendicular to the junction's axis. Several consecutive histograms were taken to verify that the histograms do not evolve under magnetic field as a function of time. Overall, we repeated the same procedure for different constant magnetic fields, starting from +1 Tesla and ending at -1 Tesla proceeding with magnetic field steps of 0.1 Tesla (e.g., Figure S5). Minus and plus signs represent magnetic fields in opposite directions. Following the described set of measurements (corresponding to the black data set in Figure 5), we immediately continued to the next set of measurements (corresponding to the red data set in Figure 5), were we repeated the described measurement procedure. However, by advancing from -1 Tesla to +1 Tesla (e.g., Figure S6).

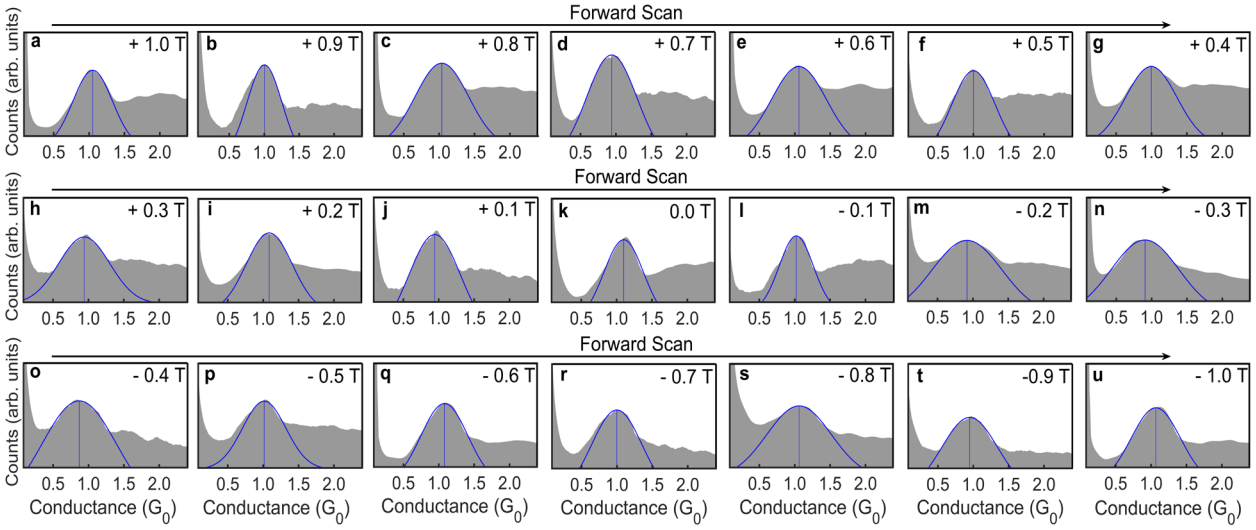

Figure S5: Conductance histograms of Fe-Ni atomic-scale junctions as a function of magnetic field applied perpendicular to the junctions. Gaussian fits and their centers are presented in blue. The extracted value of the most probable conductance by this fitting served to construct the black curve in Figure 5. Specifically, at each magnetic field presented in Figure 5, we took an average of the most probable conductance values, using Gaussian fitting to several different conductance histograms. Here, we present an example for one histogram at each field. Each conductance histogram is based on 5,000 conductance-elongation traces, at a voltage of 100 mV.

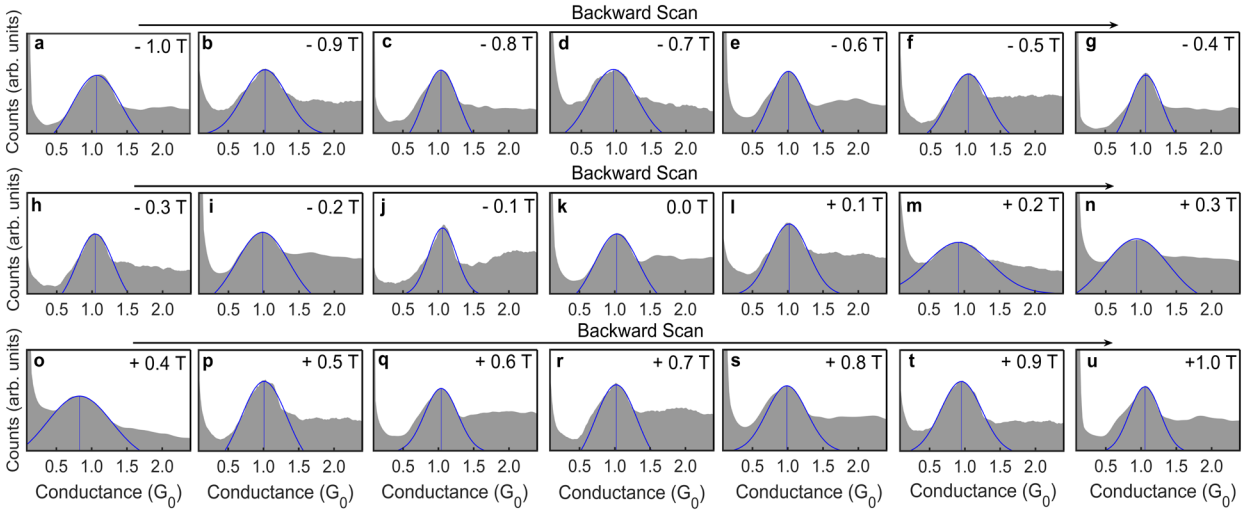

Figure S6: Conductance histograms of Fe-Ni atomic-scale junctions as a function of magnetic field applied perpendicular to the junctions. Gaussian fits and their centers are presented in blue. The extracted value of the most probable conductance by this fitting served to construct the red curve in Figure 5. Specifically, at each magnetic field presented in Figure 5, we took an average of the most probable conductance values, using Gaussian fitting to several different conductance histograms. Here, we present an example for one histogram at each field. Each conductance histogram is based on 5,000 conductance-elongation traces, at a voltage of 100 mV.

Figure S7 shows data from control experiments similar to the spin-valve measurements presented in Figure 5. Here, we repeated the same measurement procedure, however for Ni-Ni and Fe-Fe junctions. As can be seen, we did not detect the typical spin valve "butterfly" behavior. Note that the conductance response to magnetic field for Ni-Ni and somewhat for Fe-Fe is typical to anisotropic magnetoresistance[S14,S15].

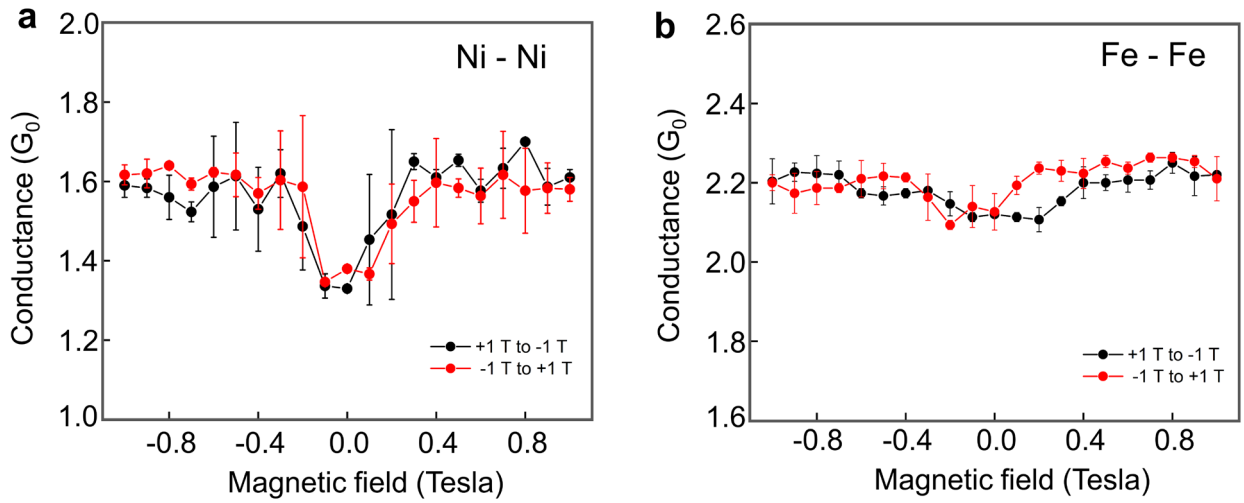

Figure S7: Conductance versus magnetic field for Ni-Ni and Fe-Fe junctions. Most probable conductance of Ni-Ni atomic junctions (a) and Fe-Fe atomic junctions (b), as a function of applied magnetic fields perpendicular to the junction axis (T denotes Tesla). The data at each magnetic field is obtained from several consecutive conductance histograms. Each histogram is based on 10,000 conductance traces measured during junction elongation, at a bias voltage of 100 mV. The error bars provide the standard deviation of the averaged data.

References:

S1. Muller, C. J.; van Ruitenbeek, J. M.; de Jongh, L. J. Experimental observation of the transition from weak link to tunnel junction. *Phys. C (Amsterdam, Neth.)* **1992**, 191, 485–504.

S2. Chakrabarti, S.; Vilan, A.; Deutch, G.; Oz, A.; Hod, O.; Peralta, J. E.; Tal, O. Magnetic control over the fundamental structure of atomic wires. *Nature Commun.* **2022**,13, 1-2 DOI:10.1038/s41467-022-31456-4

S3. Paolo, Giannozzi et al. QUANTUM ESPRESSO: a modular and open-source software project for quantum simulations of materials. *J. Phys. Condens. Matter* **2009**, 21, 395502 DOI:10.1088/0953-8984/21/39/395502

S4. Perdew, J. P.; Burke, K.; Ernzerhof, M. Generalized gradient approximation made simple. *Phys. Rev. Lett.* **1996**, 77, 3865 DOI:https://doi.org/10.1103/PhysRevLett.77.3865

S5. Smogunov, A.; Dal Corso, A.; Tosatti, E. Ballistic conductance of magnetic Co and Ni nanowires with ultrasoft pseudopotentials. *Phys. Rev. B* **2004** 70, 045417 DOI:https://doi.org/10.1103/PhysRevB.70.045417

S6. Samsonov; G. V. Handbook of the Physicochemical Properties of the Elements. Springer, **2012**.

S7. Cuevas, J. C.; Levy Yeyati, A.; Martín-Rodero, A.; Rubio Bollinger, G.; Untiedt, C.; Agraït, N. Evolution of Conducting Channels in Metallic Atomic Contacts under Elastic Deformation. *Phys. Rev. Lett.* **1998**, 81, 2990 DOI:10.1103/PhysRevLett.81.2990

S8. Jelínek, P.; Pérez, R.; Ortega, J.; Flores, F. First-principles simulations of the stretching and final breaking of Al nanowires: Mechanical properties and electrical conductance. *Phys. Rev. B* **2003**, 68, 085403 DOI: 10.1103/PhysRevB.68.085403

S9. García-Suárez, V. M.; Rocha, A. R.; Bailey, S. W.; Lambert, C. J.; Sanvito, S.; Ferrer, J. Conductance Oscillations in Zigzag Platinum Chains. *Phys. Rev. Lett.* **2005**, 95, 256804 DOI:10.1103/PhysRevLett.95.256804

S10. Vardimon, R.; Yelin, T.; Klionsky, M.; Sarkar, S.; Biller, A.; Kronik, L.; Tal, O. Probing the Orbital Origin of Conductance Oscillations in Atomic Chains. *Nano Lett.* **2014**, 14 (6), 2988–2993, DOI: 10.1021/nl4041737

S11. Krans, J. M.; Muller, C. J.; Yanson, I. K.; Govaert, T. C. M.; Hesper, R.; van Ruitenbeek J. M. One-atom point contacts. *Phys. Rev. B* **1993**, 48, 14721– 14724 DOI:10.1103/PhysRevB.48.14721

S12. Scheer, E.; Joyez, P.; Estève, D.; Urbina, C.; Devoret, M. H. Conduction Channel Transmissions of Atomic-Size Aluminum Contacts *Phys. Rev. Lett.* **1997**, 78, 3535– 3538 DOI: 10.1103/PhysRevLett.78.3535

S13. Vardimon, R.; Klionsky, M.; Tal, O. Experimental determination of conduction channels in atomic-scale conductors based on shot noise measurements *Phys. Rev. B* **2013**, 88, 161404 DOI:10.1103/PhysRevB.88.161404

S14. Bolotin, K. I.; Kuemmeth, F.; Ralph, D. C. Anisotropic Magnetoresistance and Anisotropic Tunneling Magnetoresistance due to Quantum Interference in Ferromagnetic Metal Break Junctions, *Phys. Rev. Lett.* **2006**, 97, 127202 DOI:10.1103/PhysRevLett.97.127202

S15. Keane, Z. K.; Yu, L. H.; Natelson, D. Magnetoresistance of atomic-scale electromigrated nickel nanocontacts, Appl. Phys. Lett. 2006, 88, 062514 DOI:10.1063/1.2172232